Subsonic Wing Rock of Slender Delta Wings

P. Konstadinopoulos,* D. T. Mook,† and A. H. Nayfeh‡
Virginia Polytechnic Institute and State University, Blacksburg, Virginia

Two recent experimental studies investigated the self-excited motion of a flat delta wing that was free to roll about an axis parallel to its midspan chord. In this paper these experiments are simulated numerically. An unsteady vortex-lattice method is used to provide the aerodynamic loads and the equation of motion is integrated by a prediction-correction scheme. The solution provides complete histories of the motion of the wing and the flowfield simultaneously, fully accounting for dynamic-aerodynamic interaction. The present simulation predicts that the symmetric configuration of the leading-edge vortex system becomes unstable as the angle of attack increases. Sequential views of the computed, time-dependent shape of the leading-edge system show how this causes a loss of roll damping at small angles of roll. Consequently, at sufficiently high incidence, small disturbances introduced into the flowfield grow, causing wing rock to develop. For angles of attack at onset and the amplitudes and periods of the ensuing limit cycles, the numerical predictions and experimental observations are in agreement. The simulation shows the influence of the experimental parameters and provides an explanation for the differences in the observations.

Nomenclature

a = amplitude of limit cycle
c = wing chord
C_ℓ = rolling moment coefficient
C_m = pitching moment coefficient
C_n = normal force coefficient
C_1 = dimensionless coefficient defined in Eq. (3a)
C_2 = dimensionless damping coefficient defined in Eq. (3b)
d = distance of axis of rotation below midspan chord
I = moment of inertia of wing and moving parts of sting about axis of rotation
k = reduced frequency
L = characteristic length, chord of rectangular elements in bound portion of vortex sheet
S = area of planform
t = time
T = period of limit cycle
U_∞ = freestream speed
α = angle of attack
μ = damping coefficient for bearings in sting
ρ = air density
ϕ = roll angle
τ = dimensionless time defined in Eq. (3c)

Introduction

IN parts of their flight envelopes, some highly swept delta wings operate at subsonic speeds and high angles of attack. The maximum angle of attack is often restricted by the onset of wing rock (a mainly rolling motion) instead of the occurrence of stall. Nguyen et al.[1] conducted an experimental study using a flat delta wing with 80-deg leading-edge sweep. The model was subjected to static, forced-oscillation, and free-to-roll tests. In the free-to-roll tests, the model was supported on a sting consisting of two concentric barrels separated by ball bearing assemblies and placed in a low-subsonic, steady stream in a large wind tunnel. The angle of attack was varied. The critical angle of attack at the onset of wing rock was noted and the amplitudes and periods of the ensuing limit cycles were measured. Subsequently, Levin and Katz[2] conducted a similar experiment.

There are some important differences in the two experiments. Nguyen et al. supported their model in such a way that the axis of rotation was 2 in. below the midspan chord; Levin and Katz had their axis of rotation on the midspan chord. As a result, the sideslip was different. Moreover, the size of the models, the speed of the airstream, and most likely the friction in the bearings were different. As the present results show, these are important differences.

In order to make the axis of rotation coincide with the midspan chord, Levin and Katz housed the bearing assembly inside a rather large hump or bulge along the centerline of the wing. Nguyen et al. had their bearing assembly well aft and below the wing. These differences have been the source of some controversy and speculation. Unfortunately, the present numerical simulation does not provide any information or insight on the matter.

At very large angles of attack, the leading-edge vortex systems become unstable and a phenomenon known as vortex bursting, or vortex breakdown, occurs. The discrete-vortex model apparently does not imitate the physics of the flow very well after bursting occurs. But the 80-deg-sweep delta wings used in the experiments experience wing rock well before bursting occurs.

The present simulation does show that the symmetric configuration of the leading-edge vortex system is unstable above a critical angle of attack. This causes a loss of roll damping at small angles of roll. Consequently, small disturbances introduced into the flowfield grow, causing wing rock to develop.

There are many discussions of wing rock in the literature. Several additional citations are contained in Refs. 1 and 2 as well as in a recent paper by Ericsson.[3] A comprehensive discussion can be found in the thesis by Konstadinopoulos.[4]

Numerical Model

The wing being considered is represented schematically in Fig. 1. This wing has one degree of freedom. The dynamical system includes the wing (a flat uniform plate) and the parts of the sting that rotate with it. When $d \neq 0$ the schematic drawing

Received May 1, 1984; revision received Nov. 14, 1984; presented as Paper 85-0198 at the AIAA 23rd Aerospace Sciences Meeting, Reno, Nev., Jan. 14-17, 1985.

*Graduate Research Assistant.

†Professor of Engineering Science and Mechanics.

‡University Distinguished Professor.

resembles the wing of Nguyen et al.[1] and when $d=0$ it resembles the wing of Levin and Katz.[2]

The equation of motion has the form

$$I\ddot{\phi} = (\tfrac{1}{2}\rho c S U_\infty^2) C_\ell(\phi,\dot{\phi};\alpha,d) - \mu\dot{\phi} \tag{1}$$

In both experiments, the centers of mass lay on the axis of rotation and hence there is no term in Eq. (1) for the static moment of the weight. Equation (1) can be expressed in dimensionless form as

$$\phi''(\tau) = C_1 C_\ell(\phi,\phi';\alpha,d/L) - C_2\phi' \tag{2}$$

where

$$C_1 = \rho c S L^2/8I \tag{3a}$$

$$C_2 = \mu L/2U_\infty I \tag{3b}$$

$$\tau = 2U_\infty t/L \tag{3c}$$

The coefficient C_ℓ is computed by the unsteady vortex-lattice method (UVLM) developed by Konstadinopoulos et al.[5] Using this method, one considers the wing and the wake adjoining its leading and trailing edges to be a sheet of vorticity. The portion of the sheet representing the wing is called bound, while that representing the wake is called free. Starting from known initial conditions, which must include a complete description of the wake (vorticity distribution and position) as well as the position and velocity of the lifting surface, one can march forward in time when the motion of the wing is given, calculating the generalized forces on the bound portion and describing the wake at each step. The wake is placed in the force-free position. The computations are simplified by approximating the entire vortex sheet with a lattice of discrete vortex lines.

The innovation in the present paper is to couple the UVLM with the equation of motion and to predict the motion and flowfield simultaneously and interactively.

In the simulation the wing is always given an initial displacement, held until a steady state develops and then released from rest. Hence, the initial conditions for the lifting surface always have the form

$$\phi(0) = \phi_0 \text{ and } \dot{\phi}(0) = 0 \tag{4}$$

After release the equation of motion is integrated numerically using a prediction-correction method[6]; the UVLM is a subroutine called to supply the aerodynamic loads.

Numerical Simulation of Wing Rock

In this section we consider two examples; they correspond to the experiments of Nguyen et al.[1] (case A) and Levin and Katz[2] (case B). The physical parameters of the two cases are given in Table 1. In the experiments, no attempts were made to measure the damping in the bearings of the stings. As a result, several values of C_2 in Eq. (2) are used in the numerical simulation to determine the effect of damping. The value of d is also varied in the simulation.

Table 1 Experimental parameters

	Case A Nguyen et al.[1]	Case B Levin and Katz[2]
c,m	1.765	0.429
L,m	0.442	0.107
S,m^2	0.5491	0.0321
I,kg·m^2	9.18×10^{-2}	2.7×10^{-4}
d,in.	2	0
ρ,kg/m^3	1.187	1.2
U_∞,m/s	9.266	15
C_1	0.31	0.088

In both experiments, the wings were placed in a steady stream and the angles of attack were increased until a rolling motion developed spontaneously. In both numerical simulations, the wings were given an initial displacement, held until a steady state developed, and then released from rest. The ensuing motion determines whether the wing is stable at that angle of attack.

Case A

Typical results for a stable angle of attack are shown in Fig. 2. These results describe the motion for an initial displacement of 5 deg when the angle of attack is 16 deg. In Fig. 2a, $\dot{\phi}$ is plotted as a function of ϕ (the phase plane); while in Fig. 2b, the roll angle ϕ is plotted as a function of time. The motion clearly decays and the phase plane resembles that of a stable focus. The choice of C_2 is discussed below.

Typical results for an unstable angle of attack are shown in Fig. 3. The results describe the motion for an initial displacement of 5 deg when the angle of attack is 27 deg. The same C_2

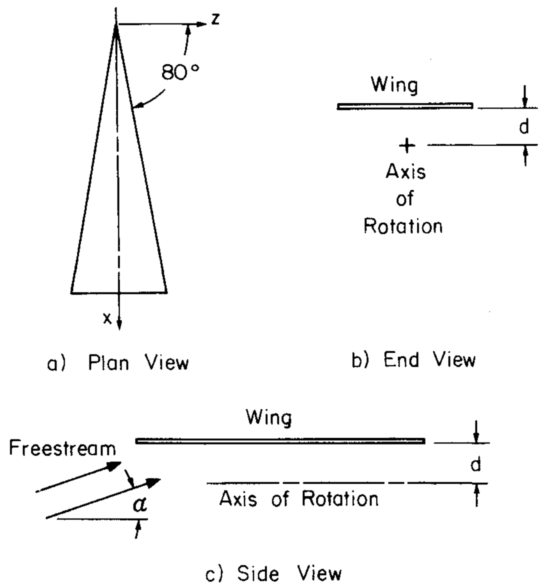

Fig. 1 Schematic of the delta wing.

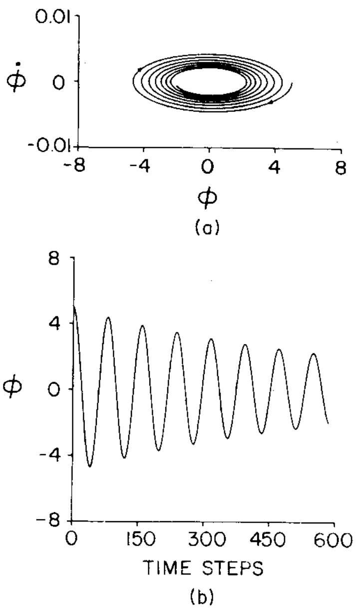

Fig. 2 Response to an initial disturbance at a stable angle of attack ($\alpha = 15$ deg), case A.

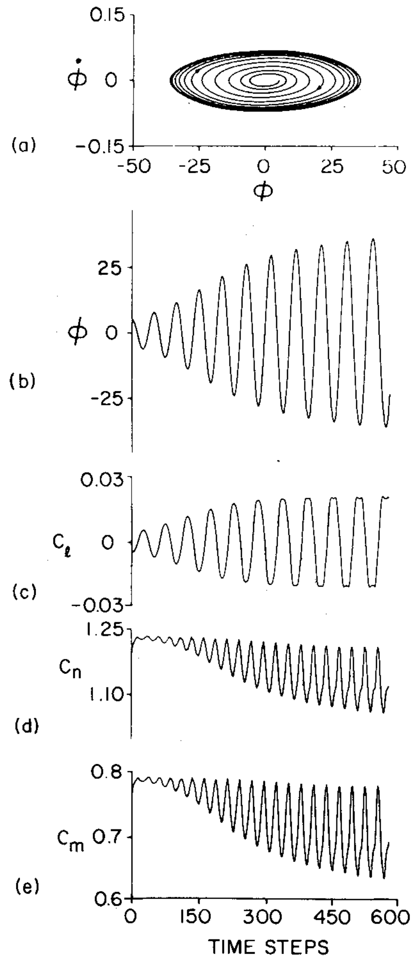

Fig. 3 Response to an initial disturbance at an unstable angle of attack ($\alpha = 27$ deg), case A.

Table 2 Effect of distance d on limit cycle for 27-deg angle of attack for case A

d, in.	0	2	4
a, deg	41	35	28
T, s	1.57	1.4	1.31
k	0.13	0.15	0.16

is used in Figs. 2 and 3. These numerical results closely resemble the observations of Nguyen et al.[1] Although the angles of attack are different in Figs. 2 and 3, the periods of the motion are nearly the same.

Nguyen et al. found the amplitude and period of the motion to be 34 deg and 0.98 s. Experimenting with different choices for C_2, we found 35 deg and 1.2 s when $C_2 = 0.01$. Moreover, this value of C_2 leads to good agreement with both the observed amplitude and period for all cases measured by Nguyen et al. More is said about C_2 below.

The period of the rolling moment is the same as that of the motion, but the period of the normal force and pitching moment is exactly half the period of the motion, as one would expect. The mean values of the pitching moment and normal force drop as the limit cycle develops.

The intersection of the envelope of the leading-edge vortex systems with a Trefftz plane just before the trailing edge is shown in Fig. 4 at various positions through half of the limit cycle. The small circles represent the streamwise, discrete-vortex lines. Also shown is the view down the perpendicular to the wing. Comparisons with wind tunnel data for steady flows showed that six streamwise vortex lines in each leading-edge

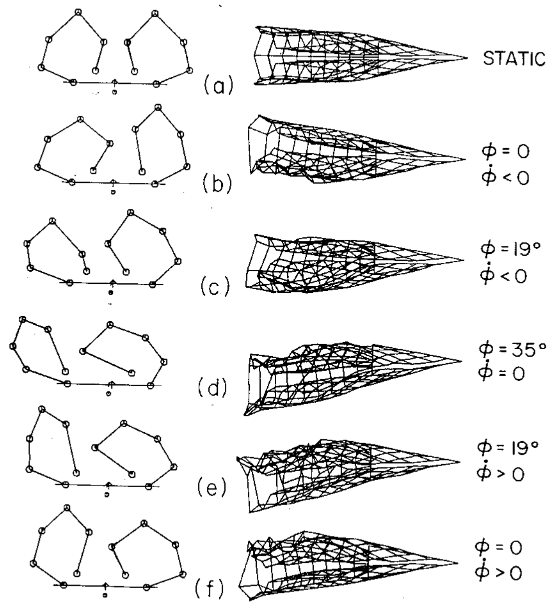

Fig. 4 Wake envelopes viewed in a Trefftz plane near the trailing edge and along the perpendicular to the wing.

system provided accurate predictions for the normal force, pitching moment, and rolling moment. The results for steady flow are shown in Fig. 4a.

Using Fig. 4, one can arrive at the following description of the wing-rock phenomenon. At small angles of roll, the motion causes the vortex system adjoining the upward-moving side to compress and the vortex system adjoining the downward-moving side to stretch. The spanwise positions of their cores remain nearly the same (Fig. 4b). As a result, the vorticity induces a larger velocity on the upward-moving side, generating a rolling moment in the direction of the rotation—a destabilizing moment. As the roll angle increases, the relative direction of the incoming stream changes, blowing the compressed vortex system outboard and the stretched system inboard (Figs. 4c and 4d). As the vortex system moves outboard, the tangential component of the velocity that it induces on the wing decreases and the normal component increases. The latter is a downwash and reduces the effective angle of attack. Eventually, the moment becomes stabilizing, the rotation stops, and the wing starts to rotate back toward its (unstable) equilibrium position.

The top views show that the side of the vortex system being compressed tends to collapse and become a little confused. This can lead to small numerical aberrations and is probably responsible for the small "teeth" in the rolling moment shown in Fig. 3. The time step was reduced by a factor of one-half twice. To two significant figures, the results were the same; however, the aberrations are less for the small time steps.

Because the wing is rotating in different directions, the positions of the leading-edge vortex systems are different in Figs. 4c and 4e (ϕ is 19 deg in both). As a result, the rolling moments are different in the two cases and hence there is hysteresis. In Fig. 5 the moment is plotted as a function of position. The arrows indicate the motion of the representative point as time increases. Hysteresis is clearly evident.

When the angle of attack is sufficiently small and wing rock does not develop, the vortex systems adjoining the leading edges lie closer to the surface of the wing than those represented in Fig. 4. As a result, the motion forces the compressed vortex above the upward-moving side more outboard than the one represented in Fig. 4b, the induced velocity is greater on the downward-moving side instead of the upward-moving side, and the direction of the moment is opposite to the direction of the motion. Consequently, there is damping, the initial disturbances decay, and the wing is stable.

The effect of the distance between the midspan chord and the axis of rotation (d) on the amplitudes and periods of the limit cycles is given in Table 2. C_2 is zero and α is 27 deg. As d increases, both the amplitude and the period decrease.

Case B

Here we simulate the experiment of Levin and Katz[2] and discuss some features of the wing-rock phenomenon and some factors affecting the experiments.

Typical results for wing rock are shown in Fig. 6. The initial angle of roll is 5 deg and the angle of attack 25 deg. The calculated form of the rolling moment as a function of time differs somewhat from that predicted in case A. Here d is zero and hence the side slipping motion is less than that in case A. As a result, the discrete vortex lines in the wake do not become quite so confused; consequently, there are smaller numerical aberrations and virtually no "teeth" in the moment. Again, the trend is for the mean values of pitching moment and normal force (not shown) to decrease as the limit cycle becomes established.

Levin and Katz observed an amplitude of 33 deg and a period of 0.4 s when α is 25 deg. Using $C_2 = 0.004$, we predict an amplitude of 32 deg and a period of 0.39 s. Again, one value of C_2 leads to close agreement for both the amplitude and period.

The effect of the damping in the bearing is shown in Table 3. The amplitudes and periods of the limit cycles are given for various values of C_2 when α is 25 deg. As C_2 increases, both the amplitude and the period decrease. When C_2 is above 0.011 approximately, wing rock does not develop from a small initial displacement at this angle of attack.

The initial displacement can affect the response. It appears from numerical experimentation that at angles of attack slightly below the threshold ($\alpha \simeq 18$ deg in the numerical simulation), small initial displacements decay while large initial displacements can lead to limit-cycle behavior. However, near the critical value of the angle of attack, changes occur very slowly in the numerical simulation and it is possible that the numerical results are misinterpreted. Nevertheless, this result is consistent with the findings of Levin and Katz.[2] They observed that when α was approximately 18 deg wing rock did not develop spontaneously, but could be produced (or maintained) by slowly decreasing α from a position where wing rock had already developed.

Table 3 Effect of bearing friction on limit cycle for $d = 0$ and 25-deg angle of attack for case B

C_2	a, deg	T, s	k
0.003	35	0.40	0.45
0.004	32	0.39	0.46
0.005	30	0.38	0.48
0.006	28	0.36	0.49
0.007	25	0.35	0.51
0.008	23	0.34	0.52
0.009	21	0.33	0.53
0.010	19	0.33	0.54
0.011	16	0.32	0.56
0.012	0	-	-

When α is 25 deg, numerical experimentation shows that the same limit cycle develops over a wide range of initial displacements. But, for initial displacements above a certain value, the motion does not become oscillatory; instead, the wing rotates continuously in one direction. This phenomenon is sometimes called roll divergence. In Fig. 7, the phase plane represents the motions for the two initial conditions. When the initial angle of roll is 45 deg, wing rock develops. The limit cycle is exactly what develops when the initial angle is 5 deg (the scales are different in Figs. 6 and 7). When the initial angle is 60 deg, the wing rolls continuously in one direction and roll divergence develops. These results suggest that between the angles of 45 and 60 deg there exists an unstable limit cycle.

The same value of C_2 that leads to close predictions of the amplitude and period when α is 25 deg also leads to a fairly good prediction of the threshold α. However, near threshold and for α of 30 deg and more, the predicted period and amplitude are not in close agreement with the observations. Near threshold this could be the result of the hump along the midspan chord, which houses the bearing assembly and is not taken into account by the present numerical model. For α of 30 deg and above, the disagreement is very likely the result of vortex bursting, which creates a damping effect that the present numerical model cannot imitate. At these high angles of attack, the observed amplitudes and periods are lower than the predictions; this is consistent with the addition of damping to

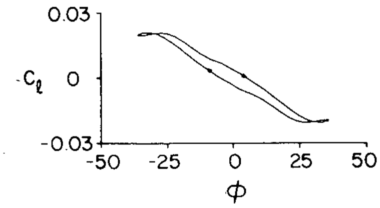

Fig. 5 Rolling moment vs angle of roll showing hysteresis.

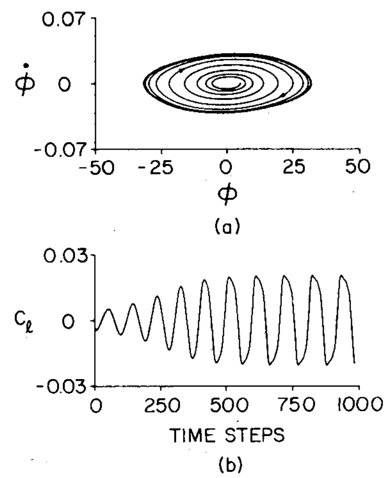

Fig. 6 Response to an initial disturbance at an unstable angle of attack ($\alpha = 25$ deg), case B.

Table 4 Coefficients a_i at various angles of attack for case B ($C_2 = 0.004$)

	(Coefficient α, deg) 10	15	20	25
a_1	−0.0047	−0.0128	−0.0351	−0.0572
a_2	−0.0143	0.0128	0.0847	0.1362
a_3	−0.0217	−0.0482	−0.0089	0.0514
a_4	0.2118	0.1646	−0.2555	−1.4030
a_5	0.2599	−0.4407	0.5530	7.9430
a_6	0.1539	0.1940	0.0588	0.0750
a_7	−3.7460	0.7672	−0.0605	1.4808

the system and counter to the trend shown by the observations at low angles of attack.

An analytical model of the aerodynamic moment can contribute to understanding wing rock. Accordingly, we represent the rolling moment with the following expansion in terms of angle of roll ϕ and roll rate $\dot{\phi}$:

$$\begin{aligned} C_\ell = {} & a_1\phi + a_2\dot{\phi} + a_3\phi^3 + a_4\phi^2\dot{\phi} \\ & + a_5\dot{\phi}^2\phi + a_6\dot{\phi}^3 + a_7\phi^5 + a_8\phi^4\dot{\phi} + a_9\phi^2\dot{\phi}^3 \\ & + a_{10}\dot{\phi}^2\phi^3 + a_{11}\phi^4\dot{\phi} + a_{12}\dot{\phi}^5 \end{aligned} \tag{5}$$

The coefficients a_i, which are functions of the angle of attack, are determined by a least-squares fit with the numerical results. It turns out that not all of the terms are important: some make virtually no contribution and their coefficients can be set equal to zero. The remaining coefficients are given for various angles of attack in Table 4. The apparent erratic behavior of a_5, a_6, and a_7 suggests that the corresponding terms are probably contributing only marginally.

It is possible to separate C_ℓ into restoring and damping components, which are defined as follows:

$$C_R = a_1\phi + a_3\phi^3 + a_5\dot{\phi}^2\phi + a_7\phi^5 \tag{6}$$

$$C_D = a_2\dot{\phi} + a_4\phi^2\dot{\phi} + a_6\dot{\phi}^3 \tag{7}$$

Referring to Table 4, we see that the coefficient of the principal restoring term a_1 is always negative and decreases as α increases. In contrast, the coefficient of the principal damping term a_2 increases and changes sign as α increases. Thus, at least at small angles of roll, the damping component changes sign and becomes destabilizing. This loss of roll damping causes wing rock to develop from small initial disturbances. In the equations governing the motion, a_2 combines with C_2 and the wing is unstable to small disturbances when the sum is positive. It is interesting to note that the trend for a_4 is opposite the trend for a_2.

More insight into the character of the total moment can be gained from Figs. 8 and 9. In Figs. 8a and 8b, the restoring component C_R and the angle of roll ϕ are plotted as functions of time when the angle of attack is 10 and 15 deg, respectively. Both are stable. In Figs. 8c and 8d, α is 20 and 25 deg, respectively. Both are unstable. The component C_R is always out of phase with ϕ and hence is always stabilizing. As the amplitude of the roll moment increases, the nonlinear effects flatten the moment curve, leaving small peaks just before and after the maximum displacement.

In Figs. 9a and 9b, the total damping moment, $C_D - C_2\dot{\phi} = C_D^*$, and $\dot{\phi}$ are plotted as functions of time when α is 10 and 15 deg, respectively. In Fig. 9b, the damping moment shows some leveling near the zeros of $\dot{\phi}$. This is an early manifestation of the loss of roll damping that develops as α increases. In Figs. 9c and 9d, α is 20 and 25 deg. In these figures,

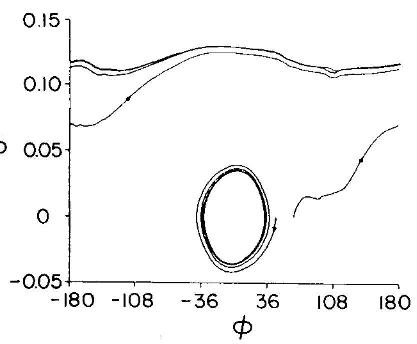

Fig. 7 Rate of roll vs angle of roll for different initial conditions, showing development of limit cycle and divergence.

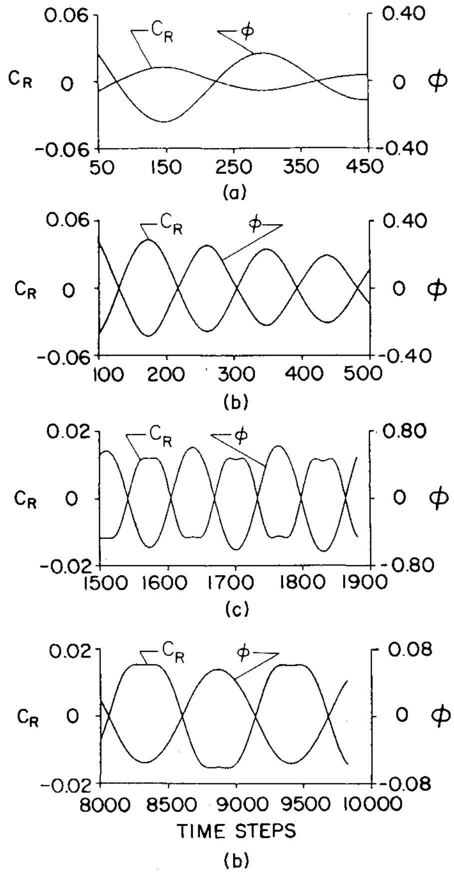

Fig. 8 Restoring component of aerodynamic moment and angle of roll vs time: a) angle of attack α is 10 deg (stable); b) $\alpha = 15$ deg (stable); c) $\alpha = 20$ deg (unstable); and d) $\alpha = 25$ deg (unstable).

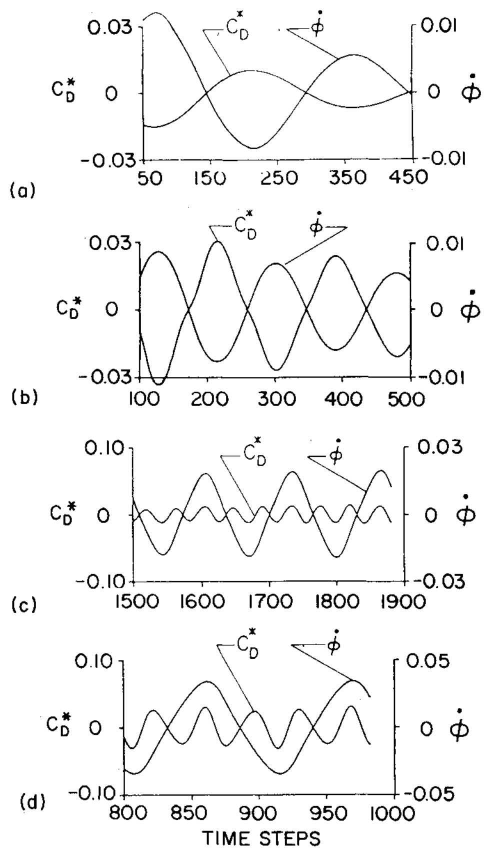

Fig. 9 Damping component of the aerodynamic moment C_D^* and rate of roll vs time: a) angle of attack α is 10 deg (stable); b) $\alpha = 15$ deg (stable); c) $\alpha = 20$ deg (unstable); and d) $\alpha = 25$ deg (unstable).

the damping moment clearly has the same sign as the velocity when the velocity is near its maximum (and ϕ is near zero) and the opposite sign when the velocity is near zero (and ϕ is near its maximum). Here, the loss of roll damping, which is responsible for wing rock, is clearly evident.

The damping changes sign relative to the velocity during a cycle, being destabilizing at small ϕ and stabilizing at large ϕ. These results suggest that there exists some similarity between this wing and the van der Pol and Rayleigh oscillators (see, e.g., Nayfeh and Mook[7]). However, the existence of a larger, unstable limit cycle between 45 and 60 deg indicates that this system is not as simple as the van der Pol and Rayleigh oscillators.

Conclusions

A numerical simulation of the subsonic wing-rock of slender delta wings has been presented. The dynamical equation governing the rolling motion of a flat delta wing about an axis parallel to its midspan chord was coupled with the unsteady vortex-lattice method. The result was integrated using a prediction-correction technique. The resulting solution yields simultaneously complete histories of the rolling motion of the wing and the flowfield, fully accounting for dynamic-aerodynamic interaction. For small angles of attack, the simulation shows that wing rock does not develop and any disturbance given to the wing decays. When the angle of attack exceeds a critical value, the present simulation predicts that the symmetric configuration of the leading-edge vortex systems becomes unstable. Sequential views of the computed, time-dependent shape of the leading-edge wake show how this causes a loss of damping at small angles of roll. As a result, small disturbances grow and the wing achieves a periodic limit cycle. Moderately large disturbances decay to the same limit cycle, in qualitative agreement with experimental observations. However, for large disturbances, the motion does not achieve a limit cycle. Instead, the wing rolls continuously in one direction, that is, roll divergence develops. It should be noted that, although the vortex-lattice method is not limited by wing planform, camber or twist, it is limited to angles of attack for which vortex bursting does not occur and to situations in which separation occurs only along the edges.

For quantitative comparison with the recent experimental results of Nguyen, Yip, and Chambers[1] and Levin and Katz[2] for free-to-roll tests of slender delta wings supported on stings, a damping term that simulates the friction in the bearings of the stings is added to the equation of motion. The simulation shows that the angle of attack at which wing rock develops and the amplitude and period of the ensuing limit cycle are strongly dependent on the magnitude of the damping coefficient in the bearings of the sting and on the location of the axis of rotation. For a given facility, a single value for the damping coefficient can be chosen such that the predicted amplitude and period are in close agreement with the observed amplitude and period.

Acknowledgment

This work was supported by the Fluid Dynamics Program of the Office of Naval Research under Contract N00014-75-C-0381, NR 061-201.

References

[1] Nguyen, L. T., Yip, L., and Chambers, J. R., "Self-Induced Wing Rock of Slender Delta Wings," AIAA Paper 81-1883, Aug. 1981.

[2] Levin, D. and Katz, J., "Dynamic Load Measurements with Delta Wings Undergoing Self-Induced Roll-Oscillations," AIAA Paper 82-1320, Aug. 1982.

[3] Ericsson, L. E., "The Fluid Mechanics of Slender Wing Rock," *Journal of Aircraft*, Vol. 21, May 1984, pp. 322-328.

[4] Konstadinopoulos, P. A., "Numerical Simulation of the Subsonic Wing-Rock Phenomenon," Ph.D. Thesis, Dept. of Engineering and Mathematics, Virginia Polytechnic Institute, Blacksburg, Va., March 1984.

[5] Konstadinopoulos, P. A., Thrasher, D. F., Mook, D. T., Nayfeh, A. H., and Watson, L., "A Vortex-Lattice Method for General, Unsteady Aerodynamics," *Journal of Aircraft*, Vol. 22, Jan. 1985, pp. 43-49.

[6] Carnahan, B., Luther, H. A., Wilkes, J. O., *Applied Numerical Methods*, John Wiley & Sons, New York, 1969.

[7] Nayfeh, A. H. and Mook, D. T., *Nonlinear Oscillations*, Wiley Interscience, New York, 1979.